

See discussions, stats, and author profiles for this publication at: <https://www.researchgate.net/publication/321500700>

Segmentation and Tracking of Inferior Vena Cava in Ultrasound Images Using a Novel Polar Active Contour Algorithm

Conference Paper · November 2017

DOI: 10.1109/GlobalSIP.2017.8309059

CITATIONS

5

READS

126

3 authors, including:



Ebrahim Karami

Memorial University of Newfoundland

72 PUBLICATIONS 714 CITATIONS

[SEE PROFILE](#)



Andrew Smith

Memorial University of Newfoundland

31 PUBLICATIONS 292 CITATIONS

[SEE PROFILE](#)

Some of the authors of this publication are also working on these related projects:



Prediction of Congestive Heart Failure Hospitalization [View project](#)



Object tracking [View project](#)

SEGMENTATION AND TRACKING OF INFERIOR VENA CAVA IN ULTRASOUND IMAGES USING A NOVEL POLAR ACTIVE CONTOUR ALGORITHM

Ebrahim Karami^{*} *Mohamed Shehata*^{*†} *Andrew Smith*[†]

^{*} Faculty of Engineering and Applied Sciences, Memorial University, St. John's, Canada

[†] Faculty of Medicine, Memorial University, St. John's, Canada

ABSTRACT

Medical research suggests that the area of the IVC and its temporal variation imaged by bedside ultrasound is useful in guiding resuscitation of the critically-ill. Unfortunately, gaps in the vessel wall and intraliminal artifact represents a challenge for both manual and existing algorithm-based segmentation techniques. In this paper, a novel polar active contour algorithm based on the third image moment is proposed and used for segmentation and tracking of the IVC in ultrasound images. To validate the proposed research in this paper, we compare the proposed algorithm with manual segmentation and three state-of-the-art relevant algorithms. It is shown that the algorithm outperforms other techniques and in some scenarios appear to have advantages over manual segmentation creating the potential to improve medical management of the critically-ill patients.

Index Terms— Inferior vena cava (IVC), ultrasound imaging, image segmentation, active contours, image moments.

1. INTRODUCTION

Accurate volume resuscitation of the critically-ill using fluids and blood products is a challenging endeavor as insufficient, excessive or delayed administration increases patient morbidity and mortality [1, 2]. Research has shown that respiratory variation in the inferior vena cava (IVC) resulting in changes in the anterior-posterior (AP) diameter is useful to predict fluid responsiveness [3, 4]. Current practice involves manual measurement of the IVC diameter and its temporal variation from ultrasound imagery however, this can be a challenging task as the image quality suffers from artifact and severe speckle noise making the vessel indistinct with unclear boundaries [5, 6]. Semi-automatic segmentation algorithms have the potential to address this issue.

Speckle noise present in ultrasound imagery is traditionally considered as Rayleigh distributed multiplicative noise [7], and hence, Rayleigh mixture models have been proposed as a potential solution for ultrasound image segmentation [8, 9]. But it has been shown that the scattering population and signal processing introduce speckle noise with non-Rayleigh distribution [10]. Furthermore, lossy compression algorithms

present on many portable ultrasound machines further deviate the recorded clip from the idealized Rayleigh distribution. In [11], it was shown that optical flow algorithms can be efficiently used for speckle tracking but this approach ignores information in vessel shape.

Active contours (AC), as planar deformable models, are widely used for segmentation of ultrasound images [12–14]. ACs perform image segmentation via minimization of an energy functional with their performance frequently dependent on a manually-defined initialization contour. In order to avoid local minima, the initiating contour needs to be as close to the actual contour as possible. ACs can be combined with other segmentation algorithms as a coarse-to-fine strategy to reduce the impact of the initial contour on segmentation error [15, 16]. Researchers [17] have approached segmenting the IVC in which the coarse segmentation obtained from template matching was smoothed with an AC (TMAC). Unfortunately, this approach fails when the IVC undergoes large frame-to-frame variations commonly present on portable machines with lower frame rates. Despite these improvements, ACs continue to perform poorly in setting of fuzzy or unclear boundaries as is commonly the case for the IVC.

Since the IVC contour is convex, polar ACs appear as a promising solution for IVC segmentation [18, 19]. In this paper, we propose a novel polar AC algorithm incorporating a novel energy functional for segmentation and tracking of the IVC in the setting of poor image quality. The proposed energy functional appears promising for other ultrasound image segmentation problems as well.

The remainder of this paper is organized as follows - Section II introduces the background and related work. The proposed polar AC algorithm is presented in Section III. The experimental results are presented in Section IV and the paper is concluded in Section V.

2. BACKGROUND AND RELATED WORK

2.1. IVC Image Structure

Fig. 1 displays a typical ultrasound image of the IVC demonstrating that the boundary is fuzzy as the cross-section of IVC does not seen as a circle. Moreover, the intravascular region



Fig. 1. A typical ultrasound image of IVC.

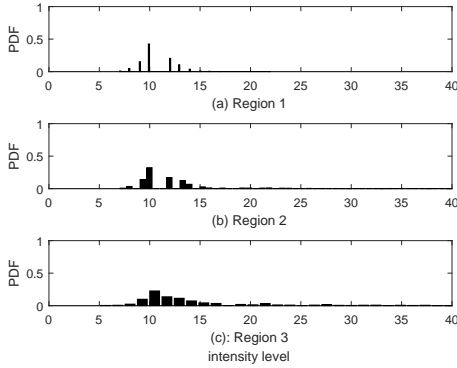


Fig. 2. PDF of the intensity levels inside the disks concentric with the IVC with radius equal to (a): 80%, (b): 100%, and (c): 120% of the IVC.

is largely hypo-echoic and extravascular hyper-echoic resulting in regional distributions with different means. Fig. 2 illustrates the probability density functions (PDFs) of the intensity levels inside the disks concentric with the IVC with diameters as (a): $D = 0.8D_{IVC}$, (b): $D = D_{IVC}$, (c): $D = 1.2D_{IVC}$, where D_{IVC} is the actual diameter of the IVC. From Fig. 2-(A) and (B), one can see that the intensity distribution inside the IVC contour is sparse. Assuming that the intensity levels inside and outside the IVC have PDFs $F_{in}(\cdot)$ with mean m_{in} and $F_{out}(\cdot)$ with m_{out} , respectively. It is clear that $m_{in} < m_{out}$ suggesting that regardless of the PDFs $F_{in}(\cdot)$ and $F_{out}(\cdot)$, their distinct means can be used for image segmentation.

2.2. Energy and Evolution Functionals

In traditional level set methods for a given energy functional $C(\cdot)$, the evolution functional is obtained as [20, 21]:

$$E \frac{\partial C}{\partial t} = -F(|\nabla C|), \quad (1)$$

where the function $F(\cdot)$ depends on the image and is usually defined as a linear function. In this paper, we use the follow-

ing linear function [20, 21]

$$E = -|\nabla C| \vec{n}, \quad (2)$$

where \vec{n} is the vector normal to the contour.

Two conventional functionals, widely employed in variational ACs, are based on the mean and the variance [22, 23]. *Functional Based on Means:* Assuming u and v represent the mean intensity levels inside and outside the IVC, respectively, the energy functional is defined as [23]

$$C_{mean} = \frac{\alpha}{2}(u - v)^2, \quad (3)$$

where α is a positive weighting factor. Using (1), the evolution functional corresponding to (3) is obtained as [23]

$$E_{mean} = \alpha(u - v) \left(\frac{I - u}{A_u} + \frac{I - v}{A_v} \right) \vec{n}, \quad (4)$$

where I is the intensity at the contour point and A_u and A_v are the areas inside and outside the contour, respectively.

Functional Based on Variances: Assuming σ_u^2 and σ_v^2 as the variances of intensity levels inside and outside the IVC respectively, the energy functional is defined as [23]

$$C_{var} = \sigma_u^2 + \sigma_v^2, \quad (5)$$

This functional is commonly used for thresholding. Using (1), the evolution functional corresponding to (5) is obtained as

$$E_{var} = \alpha \left(\frac{I^2 - u^2 - \sigma_u^2}{A_u} - \frac{I^2 - v^2 - \sigma_v^2}{A_v} \right) \vec{n}, \quad (6)$$

where u and σ_u^2 are the mean and variance of the intensities inside the contour while v and σ_v^2 represent outside the contour.

3. PROPOSED ALGORITHM

3.1. Proposed Energy Functional

The proposed functional includes the energy in the third centralized moment of the object and the curvature energy as follows

$$E = E_{M3} + E_{curv}, \quad (7)$$

where E_{M3} and E_{curv} are defined as

$$E_{M3} = -\alpha M_3, \quad (8)$$

where M_n is the n th centralized moment of the object and is obtained as

$$M_n = \frac{\int_C (I - u)^n dA}{\int_C dA}, \quad (9)$$

$$E_{curv} = \beta \sum_{n=0}^{N-1} |p_{n+1} - 2p_n + p_{n-1}|^2, \quad (10)$$

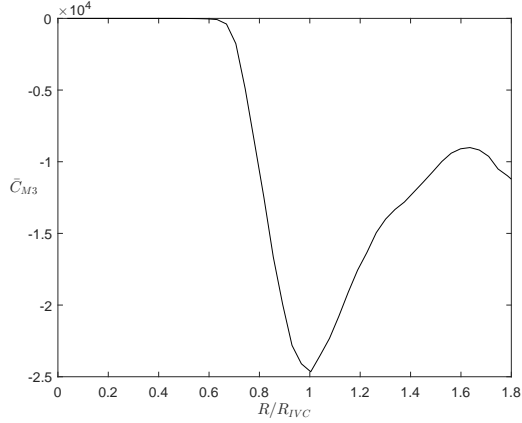


Fig. 3. E_{M3} inside a circular contour C versus the normalized radius with $\alpha = 1$.

where α and β are positive weights given to each energy term, u is the mean intensity inside the object and p_n is the point vector defined as

$$[x_c + \rho_n \cos(n\phi_0), y_c + \rho_n \sin(n\phi_0)], \quad (11)$$

with x_c and y_c being the coordinates of a point (center) inside the IVC, $\phi_0 = \frac{2\pi}{N}$, $|\nabla I|$, and ρ_n as the corresponding radial coordinate. In the rest of this section, we discuss each of these two energy terms in detail and derive their corresponding evolution functionals in the polar coordinates system.

E_{M3} energy: Fig. 3 shows the E_{M3} for the image shown in Fig. 1 with the x-axis being the normalized circle radius, R_{IVC} , and y-axis the E_{M3} inside the contour with α normalized to one. This figure shows that the E_{M3} finds its minimum at the IVC boundaries and hence is a suitable choice for the segmentation of IVC in ultrasound imagery. The gradient of E_{M3} versus $\boldsymbol{\rho} = [\rho_0, \rho_1, \dots, \rho_{N-1}]^T$ is obtained as

$$\frac{\partial E_{M3}}{\partial \boldsymbol{\rho}} = \mathbf{A}_c \boldsymbol{\rho}, \quad (12)$$

where \mathbf{A}_c is a tri-diagonal matrix defined as follows,

$$a_c(i, j) = \begin{cases} \kappa_n, & \text{if } \text{mod}(|i - j|, N) = 1, \\ 0, & \text{otherwise,} \end{cases} \quad (13)$$

with κ_n defined as

$$\kappa_n = \alpha_0 [(I(p_n) - u)^3 - M_3 - 3(I(p_n) - u)M_2], \quad (14)$$

where $\alpha_0 = -0.5\alpha \sin(\phi_0)$ and $I(p_n)$ is the pixel intensity at contour point p_n . *The curvature energy:* By substitution of (11) in (10), the curvature energy function is rewritten as

$$E_{curv} = \sum_{n=0}^{N-1} \alpha_n [4\rho_n^2 + \rho_{n-1}^2 + \rho_{n+1}^2 - 4\rho_n(\rho_{n-1} + \rho_{n+1}) \times \cos(\phi_0) + 2\rho_{n-1}\rho_{n+1} \cos(2\phi_0)], \quad (15)$$

$$\quad (16)$$

and its gradient with respect to $\boldsymbol{\rho}$ is obtained as

$$\frac{\partial E_{curv}}{\partial \boldsymbol{\rho}} = \mathbf{B}_c \boldsymbol{\rho}, \quad (17)$$

where \mathbf{B}_c is a penta-diagonal matrix defined as follows,

$$b_c(i, j) = \begin{cases} 2\beta \cos(2\phi_0), & \text{if } \text{mod}(i - j, N) = 2, \\ -8\beta \cos(\phi_0), & \text{if } \text{mod}(i - j, N) = 1, \\ 12\beta, & \text{if } i = j, \\ -8\beta \cos(\phi_0), & \text{if } \text{mod}(j - i, N) = 1, \\ 2\beta \cos(2\phi_0), & \text{if } \text{mod}(j - i, N) = 2, \\ 0, & \text{otherwise.} \end{cases} \quad (18)$$

Using (12) and (17), the energy functional in (7) can be iteratively minimized as

$$\boldsymbol{\rho}_{(i)} = \boldsymbol{\rho}_{(i-1)} - \mu(\mathbf{A}_c + \mathbf{B}_c)\boldsymbol{\rho}_{(i-1)}, \quad (19)$$

where μ is step-size parameter.

3.2. Proposed Algorithm

The proposed polar algorithm is summarized as

Table 1. Proposed Polar AC Algorithm

Input: The center of IVC in the initial frame and parameters α and β and μ and initial vector $\boldsymbol{\rho}_{(0)}$. In this research, we set them as $\alpha = 25$, $\beta = 0.025$, $\mu = 0.01$, and $\boldsymbol{\rho}_{(0)} = 12 \times \mathbf{1}_{N \times 1}$, where $\mathbf{1}_{N \times 1}$ is $N \times 1$ all-ones vector.

Step 1 - Read the first frame from the video.

Step 2 - Manually select the center of the first frame.

Step 3 - Update $\boldsymbol{\rho}$ using (19).

Step 4 - Repeat Step 3 until the algorithm reaches to the equilibrium condition. The equilibrium condition is defined as the condition where the maximum absolute value of change in $\boldsymbol{\rho}$ at the previous step is less than 10^{-3} pixels.

Step 5 - Return to step 3 for the next frame.

4. RESULTS

The experimental data was collected from two healthy subjects after ethics approval was granted. The IVC was imaged in the transverse plane using a portable ultrasound (M-Turbe, Sonosite-FujiFilm) with a phased-array probe (1-5 Mhz). Each video has a frame rate of 30 fps, scan depth of 19cm, and a duration of 15 seconds (450 frames/clip). The proposed algorithm was also compared with expert manual segmentation, two classic AC algorithms - Chan-Vese [24] and Geodesic [25], and two state-of-the-art polar ACs- PSnake [26] and variational polar AC [19]. Fig. 4 depicts the tracking performance of the investigated algorithms and compares them with

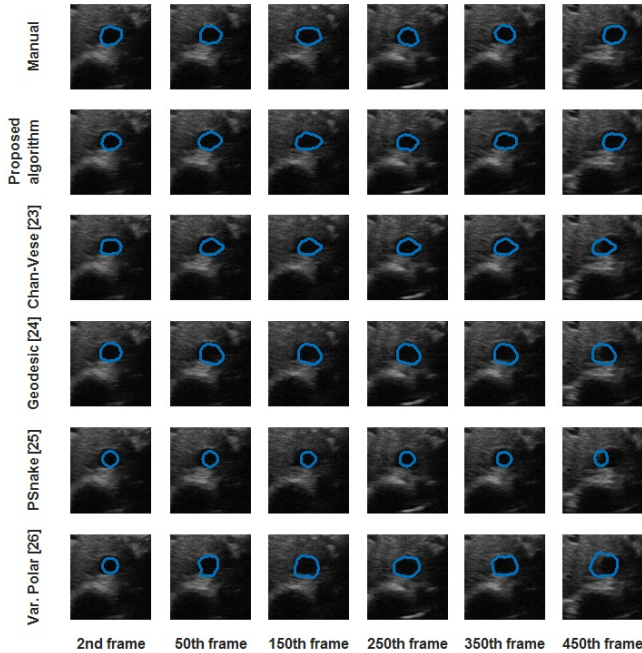


Fig. 4. Tracking of the IVC for manual segmentation, proposed algorithm and four other algorithms.

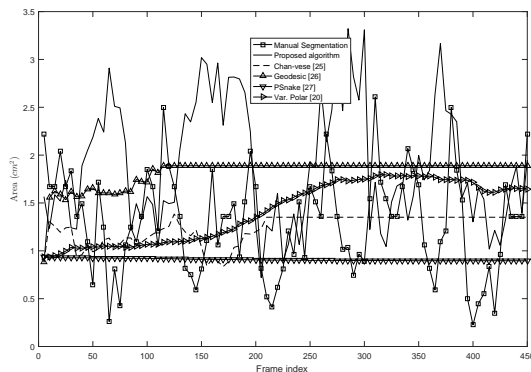


Fig. 5. IVC area (Fig 1.) as measured by the proposed algorithm, manual segmentation, and four other algorithms.

manual segmentation. As one can see from Fig. 4, except the proposed algorithm, other four algorithms are not able to track the IVC contour.

Fig. 5 presents the IVC area estimated using the proposed algorithm, manual segmentation and four other algorithms for the video depicted in Fig. 1. This confirms that only the proposed accurately tracks and segments the IVC and follows the variations in manual segmentation and other four algorithms quickly lose tracking.

Fig. 6 details the results for a lower quality IVC video. Here, it is evident that the proposed algorithm again tracks the temporal variations of the manual segmentation while other

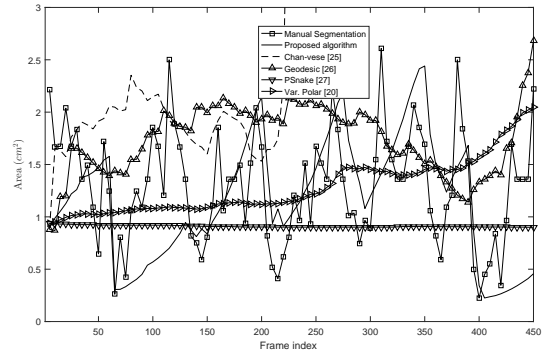


Fig. 6. IVC area as estimated by the proposed algorithm, manual segmentation, and four other algorithms.

four algorithm are unable to track the IVC.

5. CONCLUSION

In this paper, a novel polar active contour algorithm is developed for segmentation and tracking of the IVC in ultrasound imagery. A novel energy functional based on the third centralized moment of the object (in this research the area inside IVC) was proposed and used for updating polar active contour algorithm. Experimental results suggest that the proposed algorithm outperform existing segmentation algorithms and suggests improvement over manual segmentation. As the future work, the algorithm is applied for a larger dataset to explore its clinical applicability.

6. REFERENCES

- [1] V. Smyrniotis, G. Kostopanagiotou, K. Theodoraki, D. Tsantoulas, and J. C. Contis, "The role of central venous pressure and type of vascular control in blood loss during major liver resections," *The American journal of surgery*, vol. 187, no. 3, pp. 398–402, 2004.
- [2] E. Rivers, B. Nguyen, S. Havstad, J. Ressler, A. Muzzin, B. Knoblich, E. Peterson, and M. Tomlanovich, "Early goal-directed therapy in the treatment of severe sepsis and septic shock," *New England Journal of Medicine*, vol. 345, no. 19, pp. 1368–1377, 2001.
- [3] C. Charron, V. Caille, F. Jardin, and A. Vieillard-Baron, "Echocardiographic measurement of fluid responsiveness," *Current opinion in critical care*, vol. 12, no. 3, pp. 249–254, 2006.
- [4] L. Durairaj and G. A. Schmidt, "Fluid therapy in resuscitated sepsis: less is more," *Chest Journal*, vol. 133, no. 1, pp. 252–263, 2008.
- [5] W. Wang, L. Zhu, J. Qin, Y.-P. Chui, B. N. Li, and P.-A. Heng, "Multiscale geodesic active contours for ultrasound image segmentation using speckle reducing

- anisotropic diffusion,” *Optics and Lasers in Engineering*, vol. 54, pp. 105–116, 2014.
- [6] S. Sudha, G. Suresh, and R. Sukanesh, “Speckle noise reduction in ultrasound images by wavelet thresholding based on weighted variance,” *International journal of computer theory and engineering*, vol. 1, no. 1, p. 7, 2009.
- [7] R. F. Wagner, S. W. Smith, J. M. Sandrik, and H. Lopez, “Statistics of speckle in ultrasound b-scans,” *IEEE transactions on sonics and ultrasonics*, vol. 30, no. 3, pp. 156–163, 1983.
- [8] J. C. Seabra, F. Ciompi, O. Pujol, J. Mauri, P. Radeva, and J. Sanches, “Rayleigh mixture model for plaque characterization in intravascular ultrasound,” *IEEE Transactions on Biomedical Engineering*, vol. 58, no. 5, pp. 1314–1324, 2011.
- [9] M. Pereyra, N. Dobigeon, H. Batatia, and J.-Y. Tournet, “Segmentation of skin lesions in 2-d and 3-d ultrasound images using a spatially coherent generalized rayleigh mixture model,” *IEEE transactions on medical imaging*, vol. 31, no. 8, pp. 1509–1520, 2012.
- [10] T. Tuthill, R. Sperry, and K. Parker, “Deviations from rayleigh statistics in ultrasonic speckle,” *Ultrasonic imaging*, vol. 10, no. 2, pp. 81–89, 1988.
- [11] E. Karami, M. S. Shehata, and A. Smith, “Tracking of the internal jugular vein in ultrasound images using optical flow,” in *Electrical and Computer Engineering (CCECE), 2017 IEEE 30th Canadian Conference on*. IEEE, 2017, pp. 1–4.
- [12] M. Kass, A. Witkin, and D. Terzopoulos, “Snakes: Active contour models,” *International journal of computer vision*, vol. 1, no. 4, pp. 321–331, 1988.
- [13] M. Talebi, A. Ayatollahi, and A. Kermani, “Medical ultrasound image segmentation using genetic active contour,” *Journal of Biomedical Science and Engineering*, vol. 4, no. 02, p. 105, 2011.
- [14] J. A. Noble, “Ultrasound image segmentation and tissue characterization,” *Proceedings of the Institution of Mechanical Engineers, Part H: Journal of Engineering in Medicine*, vol. 224, no. 2, pp. 307–316, 2010.
- [15] S. Ali and A. Madabhushi, “An integrated region-, boundary-, shape-based active contour for multiple object overlap resolution in histological imagery,” *IEEE transactions on medical imaging*, vol. 31, no. 7, pp. 1448–1460, 2012.
- [16] E. Karami, M. Shehata, P. McGuire, and A. Smith, “A semi-automated technique for internal jugular vein segmentation in ultrasound images using active contours,” in *2016 IEEE-EMBS International Conference on Biomedical and Health Informatics (BHI)*. IEEE, 2016, pp. 184–187.
- [17] K. Nakamura, M. Tomida, T. Ando, K. Sen, R. Inokuchi, E. Kobayashi, S. Nakajima, I. Sakuma, and N. Yahagi, “Cardiac variation of inferior vena cava: new concept in the evaluation of intravascular blood volume,” *Journal of Medical Ultrasonics*, vol. 40, no. 3, pp. 205–209, 2013.
- [18] T. Li, A. Krupa, and C. Collewet, “A robust parametric active contour based on fourier descriptors,” in *2011 18th IEEE International Conference on Image Processing*. IEEE, 2011, pp. 1037–1040.
- [19] M. Baust, A. J. Yezzi, G. Unal, and N. Navab, “A sobolev-type metric for polar active contours,” in *Computer Vision and Pattern Recognition (CVPR), 2011 IEEE Conference on*. IEEE, 2011, pp. 1017–1024.
- [20] C. Li, C. Xu, C. Gui, and M. D. Fox, “Level set evolution without re-initialization: a new variational formulation,” in *Computer Vision and Pattern Recognition, 2005. CVPR 2005. IEEE Computer Society Conference on*, vol. 1. IEEE, 2005, pp. 430–436.
- [21] D. Cremers, S. J. Osher, and S. Soatto, “Kernel density estimation and intrinsic alignment for shape priors in level set segmentation,” *International journal of computer vision*, vol. 69, no. 3, pp. 335–351, 2006.
- [22] A. Yezzi, A. Tsai, and A. Willsky, “A statistical approach to curve evolution for image segmentation,” in *IEEE International Conference on Computer Vision, pages xx yy, Corfu, Greece, 1999*.
- [23] A. Yezzi, L. Zöllei, and T. Kapur, “A variational framework for integrating segmentation and registration through active contours,” *Medical image analysis*, vol. 7, no. 2, pp. 171–185, 2003.
- [24] T. F. Chan and L. A. Vese, “Active contours without edges,” *IEEE Transactions on image processing*, vol. 10, no. 2, pp. 266–277, 2001.
- [25] V. Caselles, R. Kimmel, and G. Sapiro, “Geodesic active contours,” *International journal of computer vision*, vol. 22, no. 1, pp. 61–79, 1997.
- [26] A. R. De Alexandria, P. C. Cortez, J. A. Bessa, J. H. da Silva Felix, J. S. De Abreu, and V. H. C. De Albuquerque, “psnakes: A new radial active contour model and its application in the segmentation of the left ventricle from echocardiographic images,” *Computer methods and programs in biomedicine*, vol. 116, no. 3, pp. 260–273, 2014.